Phase-field modelling of diffuse fracture with FEM

Hugo M. Leão[1], Roque L. S. Pitangueira[1], Lapo Gori[1]

[1]*Dept. of Structural Engineering, University Federal of Minas Gerais*
Av. Antônio Carlos, 6627, Pampulha, Belo Horizonte, 31270-901, Minas Gerais, Brazil
hugomleao@yahoo.com.br, roque@dees.ufmg.br, lapo@dees.ufmg.br

Abstract. In damage models, cracks are considered in a smeared way, without any geometric representation of the region where the crack takes place, and the energy released is used in crack growth that is controlled by the energy fracture parameter. Phase-field models consider a diffuse and smooth crack that belongs to a certain volume region, where a function describes the crack density. In that region each point has a field variable that quantifies the material degradation. The phase-field techniques allows to detect crack paths and its bifurcation without having a pre-existent crack. The purpose of this work is to present some phase-field models implemented in the INSANE (Interactive Structural ANalysis Environment system) software, an structural analysis open-source software developed by at the Structural Engineering department (DEES) of the Federal University of Minas Gerais (UFMG). This work opens a new research line inside the INSANE Project. Some preliminary results will be presented.

Keywords: Phase-Field Cracking Models, Finite Element Method, Nonlinear Analysis, INSANE Computational System

1 Introduction

Fracture is an important failure mechanism for engineering materials and it has been extensively studied to prevent catastrophic collapse of engineering structures [1]. Griffith criterion is based on a pre-existing crack that propagates when the energy release rate matches the fracture toughness [2]. This method, however, presents a number of limitations, like the need for a pre-existing crack and the impossibility to describe curvilinear crack paths [3]. Besides overcoming these limitations, phase-field models can detect cracks bifurcation and can describe a sharp crack without the need for the geometrical representation. For that, the phase-field model incorporates a continuous field variable (ϕ) that represents a smooth transition between the completely broken and unbroken material. Another variable of the phase-field models is the length scale parameter (l_0) that relates the diffusive approximation of the sharp crack. When the parameter l_0 becomes larger, the degraded region also becomes larger.

This work presents some phase-field techniques that has been implemented in INSANE[1] (*INteractive Structural ANalysis Environment System*), an open-source software developed by the Structural Engineering Department at the Federal University of Minas Gerais.

A lot of phase-field models can be found in the literature. Bourdin et al. [5], for example, proposed an isotropic model to represent crack propagation. Anisotropic models, that separate traction and compression regions, can also be cited as, for example, the models of Lancioni and Royer-Carfagni [6] and Amor et al. [7]. It should be noted that, when dealing with phase-field models, the therms isotropic and anisotropic is not related to material proprieties, but to the separation of energy regions. In this present work, just the isotropic model will be presented once the implementation of anisotropic model is already in course.

2 Phase-field models

Phase-field models has some functions that are keys of its operation. They are the *crack surface density function* ($\gamma(\phi, \nabla\phi)$) and the *energetic degradation function* ($g(\phi)$). The function γ is responsible to give the

---

[1]More informations on the project can be found at `https://www.insane.dees.ufmg.br/`, the development code is freely available at the Git repository `http://git.insane.dees.ufmg.br/insane/insane.git`.

smeared characteristic to the crack. Wu [1] had presented a generic way to describe it:

$$\gamma(\phi, \nabla\phi) = \frac{1}{C_0}\left[\frac{1}{l_0}\alpha(\phi) + l_0|\nabla\phi|^2\right],$$ (1)

where $\alpha(\phi)$, called *geometrical crack function*, determines how phase-field will be distributed and it has to satisfy $\alpha(0) = 0$ and $\alpha(1) = 1$. The parameter C_0 is dependent on alpha by the integral: $C_0 = 4\int_0^1\alpha^{1/2}d\phi$. The function g degradates the energy. In this way, beyond deformation (ε), it is assumed that the strain energy function (ψ) depends on g, by the following form

$$\psi(\varepsilon) = g(\phi)\psi_0^+(\varepsilon) + \psi_0^-(\varepsilon),$$ (2)

where ψ_0^+ represents the part of the energy that comes from tension, and ψ_0^- from compression. It is important to emphasize that only anisotropic models makes this differentiation. In isotropic models the function g multiplies the whole elastic energy function.

There are some criteria that $g(\phi)$ must satisfy:
- $g(0) = 1$: there is no degradation in intact material;
- $g(1) = 0$: the energy is completely degraded in fully broken material;
- $g'(\phi) = \dfrac{dg}{d\phi} < 0$: the function $g(\phi)$ has to be monotonically decreasing;
- $g'(1) = 0$: there isn't sudden variation in the interface where the material in fully broken.

With all this in mind, a domain Ω with a damaged part $\mathcal{B} \subset \Omega$ is considered. The boundary of the solid and its damaged surface are, respectively, $\partial\Omega$ and $\partial\mathcal{B}$. Therefore, the total energy functional becomes:

$$E_t = \int_\Omega \psi(\varepsilon(\boldsymbol{u}), \phi)dV + \int_\mathcal{B} G_c\gamma(\phi, \nabla\phi)dV - \int_\Omega \boldsymbol{b}\cdot\boldsymbol{u}dV - \int_{\partial\Omega} \boldsymbol{t}\cdot\boldsymbol{u}dA,$$ (3)

where G_c is the fracture energy, $\boldsymbol{u}$ is the displacement vector, and $\boldsymbol{b}$ and $\boldsymbol{t}$ are, respectively, the body and surface forces.

With all of this shown above it is possible to demonstrate that the governing equations of a phase-field model in the weak form are:

$$\begin{cases}\int_\Omega \boldsymbol{\sigma} : \delta\varepsilon dV = \delta P_{ext} \\ \int_\mathcal{B}\left[g'(\phi)\bar{Y}\delta\phi + G_c\delta\gamma\right]dV \geq 0\end{cases}, \quad \text{with} \quad \delta\gamma = \frac{1}{C_0}\left[\frac{1}{l_0}\alpha'(\phi)\delta\phi + 2l_0\nabla\phi\cdot\nabla\delta\phi\right],$$ (4)

where the first equation of the system 4 is the standard weak form of classical elasticity while the second one comes from minimization of functional 3.

3 Finite element discretization

In the Finite Element Method, the displacement field, the strain field and the phase-field are interpolated from displacement ($\boldsymbol{d}$) and phase-field ($\boldsymbol{a}$) nodal values:

$$\boldsymbol{u}(\boldsymbol{x}) = \boldsymbol{N}^u\boldsymbol{d}, \quad \varepsilon(\boldsymbol{x}) = \boldsymbol{B}^u\boldsymbol{d}, \quad \phi(\boldsymbol{x}) = \boldsymbol{N}^\phi\boldsymbol{a}, \quad \nabla\phi(\boldsymbol{x}) = \boldsymbol{B}^\phi\boldsymbol{a},$$ (5)

where the matrices $\boldsymbol{N}$ and $\boldsymbol{B}$ are written using the approximation functions:

$$\boldsymbol{N}^u = \begin{bmatrix} N_i^u & 0 \\ 0 & N_i^u \end{bmatrix}, \quad \boldsymbol{B}_i^u = \begin{bmatrix} N_{i,x}^u & 0 \\ 0 & N_{i,y}^u \\ N_{i,y}^u & N_{i,x}^u \end{bmatrix}, \quad \boldsymbol{N}_i^\phi = \left\{N_i^\phi\right\}, \quad \boldsymbol{B}_i^\phi = \begin{bmatrix} N_{i,x}^\phi \\ N_{i,y}^\phi \end{bmatrix}.$$ (6)

From definitions 5 and 6, the system of equations 4 becomes:

$$\begin{cases} \int_\Omega (\boldsymbol{B}^u)^T \boldsymbol{\sigma} dV = \boldsymbol{f}_{ext} \\ \int_\mathcal{B} g' \bar{Y} (\boldsymbol{N}^\phi)^T dV + \int_\mathcal{B} \frac{G_c}{C_0} \left(\frac{1}{l_0} \alpha' (\boldsymbol{N}^\phi)^T + 2l_0 (\boldsymbol{B}^\phi)^T \nabla \phi \right) dV \geq 0 \end{cases} . \tag{7}$$

With the residual values described in 8 and stiffness matrix in 9:

$$\boldsymbol{r}^u = \boldsymbol{f}_{ext} - \int_\Omega (\boldsymbol{B}^u)^T \boldsymbol{\sigma} dV = \boldsymbol{0}, \quad \boldsymbol{r}^\phi = -\int_\mathcal{B} \left[(\boldsymbol{N}^\phi)^T \left(g' \bar{Y} + \frac{1}{C_0 l_0} \alpha' G_c \right) + \frac{2l_0}{C_0} G_c (\boldsymbol{B}^\phi)^T \nabla \phi \right] dV \leq \boldsymbol{0}. \tag{8}$$

$$\boldsymbol{K}_{element} = \begin{bmatrix} \boldsymbol{K^{uu}} & \boldsymbol{K^{u\phi}} \\ \boldsymbol{K^{\phi u}} & \boldsymbol{K^{\phi\phi}} \end{bmatrix}, \quad \boldsymbol{K_{uu}} = \int_\Omega (\boldsymbol{B}^u)^T \frac{\partial \boldsymbol{\sigma}}{\partial \boldsymbol{\varepsilon}} \boldsymbol{B}^u dV, \quad \boldsymbol{K_{u\phi}} = \int_\Omega (\boldsymbol{B}^u)^T \frac{\partial \boldsymbol{\sigma}}{\partial \phi} \boldsymbol{N}^\phi dV, \tag{9a}$$

$$\boldsymbol{K_{\phi u}} = \int_\mathcal{B} (\boldsymbol{N}^\phi)^T g' \frac{\partial \bar{Y}}{\partial \boldsymbol{\varepsilon}} \boldsymbol{B}^u dV, \quad \boldsymbol{K_{\phi\phi}} = \int_\mathcal{B} (\boldsymbol{N}^\phi)^T \left(g'' \bar{Y} + \frac{1}{C_0 l_0} \alpha'' G_c \right) \boldsymbol{N}^\phi dV + \int_\mathcal{B} \frac{2l_0}{C_0} G_c (\boldsymbol{B}^\phi)^T \boldsymbol{B}^\phi dV. \tag{9b}$$

4 Computational implementation

There are two approaches to the solution of the system of equations 7: monolithic and staggered solvers. Monolithic solver tries to solve both equation in the same iteration. Since the energy functional is not convex with respect to displacements and phase-field variables, the monolithic solver converges only in specific situations (Wu et al. [8]). Staggered solver solves the displacement and the phase-field one at a time resulting in a more robust process, and are capable to overcome some of the issues of monolithic solver. Every implementation discussed forward was done to solve plane problems and in order to make the least possible intervention in the INSANE code.

4.1 Monolithic solver

To implement the monolithic solver in INSANE system the matrices $\boldsymbol{B}$ and $\boldsymbol{C}$ (constitutive matrix) were written to addapt the phase-field theory in already existing environment. With these implementations the final stiffness matrix mounted has the same therms as the one described in equation 9. In this way, it gets:

$$\boldsymbol{C}_{tangent}^{mon} = \begin{bmatrix} \left[\frac{\partial \boldsymbol{\sigma}}{\partial \boldsymbol{\varepsilon}} \right]_{3\times3} & \left[\frac{\partial \boldsymbol{\sigma}}{\partial \phi} \right]_{3\times1} & [\boldsymbol{0}]_{3\times2} \\ \left[g' \frac{\partial \bar{Y}}{\partial \boldsymbol{\varepsilon}} \right]_{1\times3} & \left[g'' \bar{Y} + \frac{1}{C_0 l_0} \alpha'' G_c \right]_{1\times1} & [\boldsymbol{0}]_{1\times2} \\ [\boldsymbol{0}]_{2\times3} & [\boldsymbol{0}]_{2\times1} & 2\frac{l_0}{C_0} G_c [\mathbb{I}]_{2\times2} \end{bmatrix}, \quad \boldsymbol{B}_i^{mon} = \begin{bmatrix} N_{i,x}^u & 0 & 0 \\ 0 & N_{i,y}^u & 0 \\ N_{i,y}^u & N_{i,x}^u & 0 \\ 0 & 0 & N_i^\phi \\ 0 & 0 & N_{i,x}^\phi \\ 0 & 0 & N_{i,y}^\phi \end{bmatrix} . \tag{10}$$

The dual internal variable vector (σ) was already needed implement as shown in equation 11:

$$\boldsymbol{\sigma} = \begin{bmatrix} \sigma_x & \sigma_y & \tau_{xy} & g' \bar{Y} + \frac{G_c}{C_0 l_0} \alpha' & 2\frac{G_c l_0}{C_0} \phi_{,x} & 2\frac{G_c l_0}{C_0} \phi_{,y} \end{bmatrix}^T . \tag{11}$$

4.2 Staggered solver

The staggered solver solves equations 8 one at a time as a decoupled problem. For that, it is just used the stiffness matrices $\boldsymbol{K}_{uu}$ and $\boldsymbol{K}_{\phi\phi}$. In this way, to solve the problem for displacements and for phase-field, the matrices 12a and 12b were implemented, respectively, in INSANE.

$$\boldsymbol{C}_{tangent}^{stg,u} = \frac{\partial \boldsymbol{\sigma}}{\partial \boldsymbol{\varepsilon}}, \quad \boldsymbol{B}_i^{stg,u} = \begin{bmatrix} N_{i,x}^u & 0 \\ 0 & N_{i,y}^u \\ N_{i,y}^u & N_{i,x}^u \end{bmatrix}, \tag{12a}$$

$$\boldsymbol{C}_{tangent}^{stg,\phi} = \begin{bmatrix} g''\bar{Y} + \dfrac{1}{C_0 l_0}\alpha''G_c & 0 & 0 \\ 0 & 2\dfrac{l_0}{C_0}G_c & 0 \\ 0 & 0 & \dfrac{l_0}{C_0}G_c \end{bmatrix}, \quad \boldsymbol{B}_i^{stg,\phi} = \begin{bmatrix} N_i^\phi \\ N_{i,x}^\phi \\ N_{i,y}^\phi \end{bmatrix}. \tag{12b}$$

5 Obtained Results

As the present work is still ongoing, only the isotropic constitutive model has been implemented hence, all the following results were obtained with that model. All presented results were obtained using the staggered solver, once the monolithic had presented convergence issues in the softening branch of the equilibrium path. For all the examples, the functions $g(\phi) = (1 - \phi)^2$ and $\alpha(\phi) = \phi^2$ were considered. Besides the structural behaviour, also the material behaviour has been investigated for both the examples, by doing a uniaxial traction test; the maximum value of traction (f_t) was compared to a theoretical value given by equation 13 [8].

$$f_t = \frac{3}{16}\sqrt{\frac{3E_0 G_c}{l_0}} \tag{13}$$

5.1 Shear Test

The first example consists in the shear test depicted in figure 1, modelled using a mesh of 100×100 square elements, imposing a constant horizontal displacement at the nodes on the top edge. The following material parameters were adopted: $E = 210 \text{ kN/mm}^2$, $\nu = 0.2$, $G_c = 2.7 \times 10^{-3} \text{ kN/mm}$, $l_0 = 0.03 \text{ mm}$. In figure 2 the load-displacement curves for the shear test and for the uniaxial test of the material are shown.

The simulated value of f_t was 1.381 kN/mm^2, while value of equation 13 was 1.412 kN/mm^2, resulting in a difference of approximately 2.2%.

5.2 Asymmetric Tension Test

The second example is the asymmetric traction shown in figure 3, modelled using a triangular mesh refined in the region of the crack. A uniform vertical displacement was imposed at the nodes on the top edge, and the following material parameters were adopted: $E = 1 \text{ kN/mm}^2$, $\nu = 0.3$, $G_c = 1.0 \times 10^{-3} \text{ kN/mm}$, $l_0 = 0.0066 \text{ mm}$. The load-displacement curves are shown in figure 4.

The simulated value of f_t was 0.126 kN/mm^2, while value of equation 13 was 0.119 kN/mm^2, resulting in a difference of approximately 5.6%.

6 Conclusions

The present work intends to implement phase-field models on INSANE. The isotropic constitutive model were already implemented with the monolithic and staggered solver. It was very clear that INSANE is a very
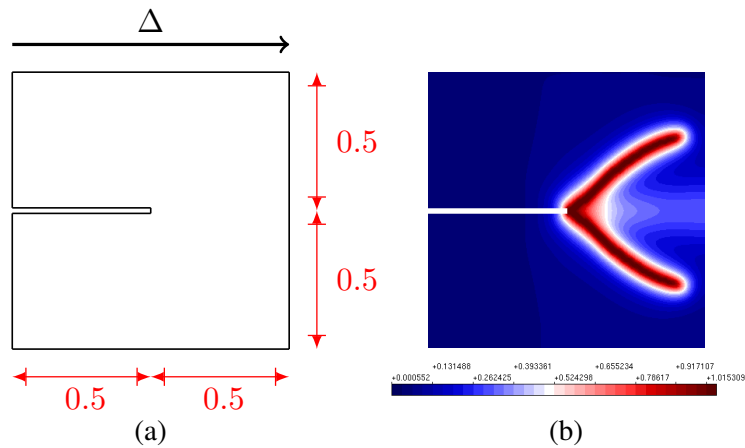
Figure 1. Shear test. All dimensions are in millimetres. (a) Problem Setting. The nodes in the bottom edge are fixed, and the nodes in the other three edges are fixed in the vertical direction. (b) Numerical results for phase-field (ϕ).
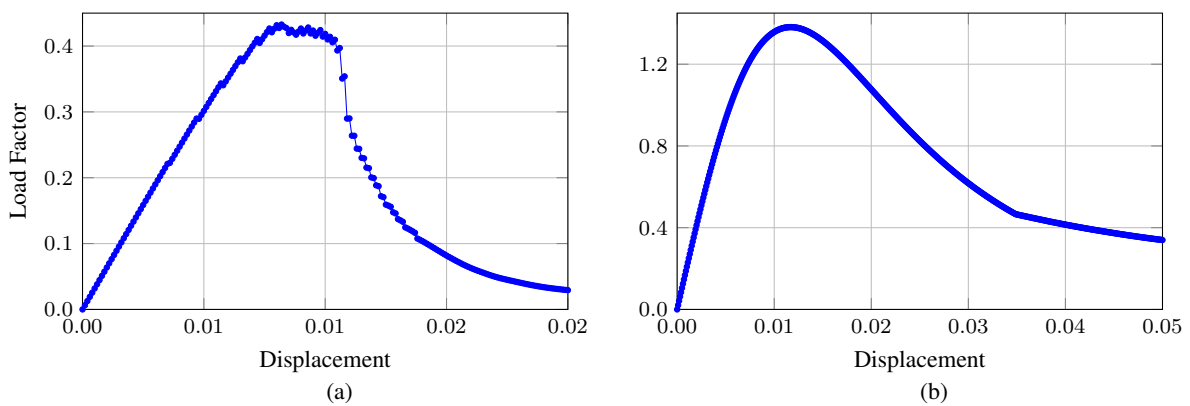

Figure 2. Load-displacement curves. (a) Top edge structural behaviour (b) Material behaviour.
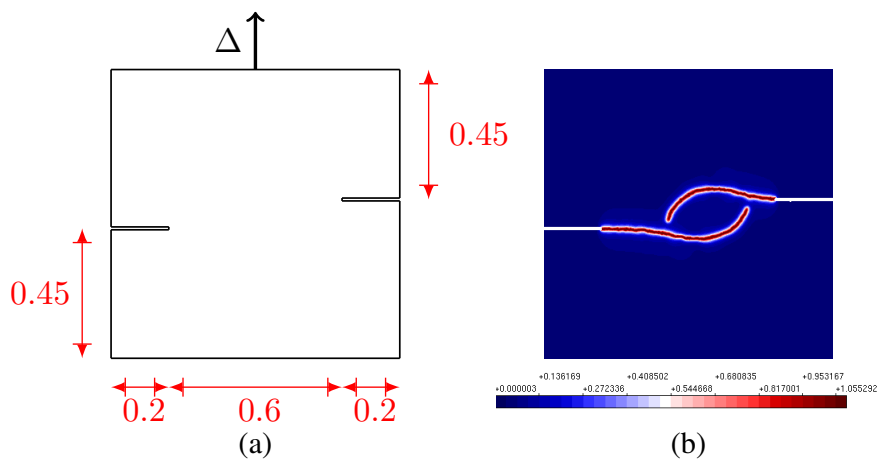

Figure 3. Tension test. All dimensions are in millimetres. (a) Problem Setting. The nodes in the bottom edge are fixed. (b) Numerical results for phase-field).

robust software and there is a great potential to implement all kinds of models due of its generalizations in code. As it was already mentioned by Wu et al. [8], the monolithic solver presents issues in convergence, and it doesn't conduces to good results. In both examples tested, it stops converges when the load factor starts to decrease. The obtained crack patters are similar to those described in the literature.
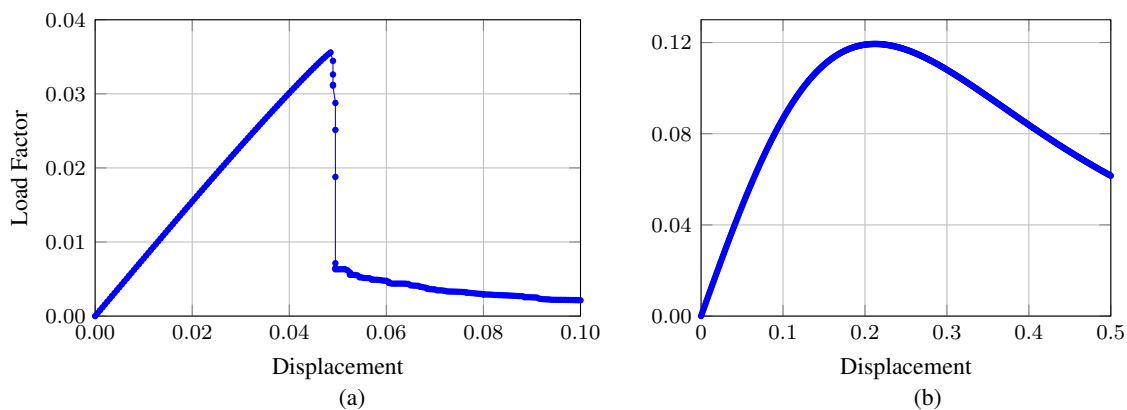
Figure 4. Load-displacement curves. (a) Top edge structural behaviour (b) Material behaviour.

Authorship statement. The authors hereby confirm that they are the sole liable persons responsible for the authorship of this work, and that all material that has been herein included as part of the present paper is either the property (and authorship) of the authors, or has the permission of the owners to be included here.

References

[1] Wu, J.-Y., 2017. A unified phase-field theory for the mechanics of damage and quasi-brittle failure. *Journal of the Mechanics and Physics of Solids*, vol. 103, pp. 72–99.

[2] Broek, D., 1984. *Elementary Engineering Fracture Mechanics*. Martinus Nijhoff Publishers.

[3] Miehe, C., Welschinger, F., & Hofacker, M., 2010. Thermodynamically consistent phase-field models of fracture: Variational principles and multi-field fe implementations. *International Journal for Numerical Methods in Engineering*, vol. 83, pp. 1273–1311.

[4] Penna, S. S., 2011. Formulação multipotencial para modelos de degradação elástica: unificação teórica, proposta de novo modelo, implementação computacional e modelagem de estruturas de concreto.

[5] Bourdin, B., Francfort, G., & Marigo, J. J., 2000. Numerical experiments in revisited brittle fracture. *Journal of the Mechanics and Physics of Solids*, vol. 48, pp. 797–826.

[6] Lancioni, G. & Royer-Carfagni, G., 2009. The variational approach to fracture mechanics. *Journal of Elasticity*, vol. 95, pp. 1–30.

[7] Amor, H., Marigo, J.-J., & Maurini, C., 2009. Regularized formulation of the variational brittle fracture with unilateral contact: Numerical experiments. *Journal of the Mechanics and Physics of Solids*, vol. 57(8), pp. 1209–1229.

[8] Wu, J.-Y., Nguyen, V. P., Thanh Nguyen, C., Sutula, D., Bordas, S., & Sinaie, S., 2019. Phase field modelling of fracture. *Advances in Applied Mechanics*, vol. 53, pp. https://www.sciencedirect.com/science/article/pii/S0065215619300134.

[9] Drucker, D. C., 1951. A more fundamental approach to plastic stress-strain relations. In *Proceedings of the First National Congress of Applied Mechanics*, pp. 487–491, Chicago, USA. ASME.

[10] Bažant, P. Z. & Lin, F. B., 1988. Non-local yield limit degradation. *International Journal for Numerical Methods in Engineering*, vol. 26, pp. 1805–1823.